Neutron radiography with simultaneous deformation measurements demand rethinking the modelling of imbibition in cement paste

Alderete Natalia Mariel[a, 1*], Villagrán – Zaccardi Yury[b], Shields Yasmina[a], Van den Heede Philip[a], Zappitelli María Paula[c], Patel Ravi[d], Jovanović Balša[a], Trtik Pavel[e], De Belie Nele[a]

[a]Magnel-Vandepitte Laboratory for Structural Engineering and Building Materials, Ghent University. Technologiepark Zwijnaarde 60, Campus Ardoyen, B-9052 Gent. Belgium. [1*] corresponding author: nataliamariel.alderete@ugent.be.

[b]Sustainable Materials, Flemish Institute for Technological Research (VITO), Boeretang 200, 2400 Mol, Belgium.

[c]Construction Department, Faculty of Engineering, National University of La Plata. Calle 1 y 47, La Plata (B1900TAG), Buenos Aires. República Argentina.

[d] Karlsruher Institute of Technology (KIT), Lieferanschrift: Geb. 50.32, Warenannahme Tor 8, Gotthard-Franz-Str. 2, 76131 Karlsruhe. Germany.

[e] Neutron Imaging and Activation Group, Laboratory for Neutron Scattering and Imaging Paul Scherrer Institut, 5232 Villigen PSI. Switzerland.

Abstract

During capillary imbibition, there are changes in the pore structure that reduce the water ingress rate, leading to anomalous behaviour. However, the relation of those deformations with the C-S-H content is still unclear. We performed simultaneous measurements of external deformations and water ingress through neutron radiography. Cement pastes of water/cement of 0.4 and 0.6, using both Portland and white cement were tested after 1 year curing. Porosity and calcium silicate hydrate (C-S-H) content of the pastes were determined. Strain gauges were attached perpendicular and parallel to the water flow. Results indicate that the degree of internal restriction of the mix influences the shape of the water profile and that C-S-H deformations affect internal changes more than external. Water ingress visualization indicated the lack of a sharp front during imbibition and the saturation degree variation at the position of the strain gauges. We propose a model to address the dynamic porosity.

1. Introduction

On the basis of unsaturated flow theory, capillary ingress can be modelled by the simple law of mass increase varying linearly with the square root of time. This is suitable for most construction materials but cementitious materials tell a different anomalous story. Water ingress in cement-based materials does not have a linear variation with the square root of time, it decelerates faster than this. A practical and improved way to describe the anomalous behaviour (and to obtain the sorptivity coefficient independent from test duration), is the fourth root of time approach [1]. This approach is based on the substantial experimental evidence [2–6] that the main cause of the anomaly is the swelling of the main compound of hardened cement paste: calcium silicate hydrate (C-S-H). C-S-H has a hygroscopic nature, it deforms in contact with water and changes the pore size distribution of the cementitious matrix during imbibition.

The big question of why capillary absorption of water by cement paste is still not addressed as an imbibition process (thus considering swelling) may still be based on the presumption that the properties of C-S-H do not transfer as such to cement paste as a whole. There are tremendous indications consistent with the assumption of cement paste as a deformable solid, such as the development of drying shrinkage and creep. But other phases and pores are also present in cement paste, and as a result, C-S-H deforms

experiencing internal restrictions. The degree to which those deformations lead to expansion of cement paste or to a decrease in hydraulic diffusivity is still a matter of research.

Measurements of external deformations caused by swelling can provide new insights into the transport process. Volumetric changes evidence a dynamic pore structure during water ingress, as already measured in paste[7], mortar [8] and concrete [8]. The influencing factors leading to synchronous strains seem to be the relative amount of porosity and deformable phases. This is an interesting link between the changes at nano- and microscale and the changes at macroscale. Similarly, Chemmi H. et al.[9] describe the importance of the connection between the different scales. They argue that, at nano-scales, the water molecule dynamics is fully restricted by the proximity of the pore surfaces. Instead, at micro-, meso- and macro- scales, R.H. is a relevant parameter for controlling the dynamics of confined water. Particularly at meso-scales, the wettability on the interface considerably impacts the water dynamics; and at macro-scales, connectivity and tortuosity reveal that the geometry is of primary importance for moisture transport [9]. The evidence supporting the fact that cementitious materials experience a dynamic porosity during water ingress is extensive. Jiang et al.[10] studied the pore size distribution of saturated cement paste samples and concluded that the swelling of the C-S-H sheets led to a decrease in the volumes of gel pores. Using single-sided 1H nuclear magnetic resonance (NMR), Holthausen and Raupach[11] analysed the porosity changes of mortar samples that were dried and rewetted. They found a temporary decrease of C-S-H interlayer signal due to fast swelling of the dried-up gel pore spaces. Several other NMR based studies detected pore changes during water ingress [10–14]. Still, it is debatable what could be considered as "C-S-H swelling". Perhaps the term is not specific to one phenomenon and it is possible that is not the only cause of anomalous imbibition. However interesting, this nature of "swelling" is not the main focus of this paper. Their effects, i. e. volumetric changes, are studied here. From the external deformation measurements, the volumetric changes can be connected to the changes inside the pore structure. Additionally, determining the external deformations simultaneously with water ingress visualisation can help to better describe the water transport.

Neutron radiography provides high spatial resolution and extraordinary sensitivity to water content. Neutron attenuation enables measuring the moisture content in cement-based materials, as neutrons are strongly attenuated by the hydrogen present in water and relatively insensitive to the other components in cementitious materials[15]. Imbibition in mortars was successfully analysed by neutron radiography in previous research[16–20], but using mortar (instead of paste) can lead to high noise levels in the resolved moisture profiles due to differences in moisture content between the aggregates and the matrix. Hence, for this study paste samples were chosen to increase accuracy in the image analysis. Neutron radiography was used to determine the spatial and time dependent water distribution during imbibition for 5 h with synchronous deformation measurements. Therefore, the swelling effect was studied along with simultaneous visualisation of the shape and position of the water front during imbibition.

Traditionally, to predict moisture distribution in porous materials, models based on the extended Darcy or Fick's law with empirical nonlinear diffusion coefficient for moisture diffusion are used[21,22]. Alternatively, simplification to Darcy's law can be made by assuming constant gas pressure which leads Richards' equation that has also been used to predict capillary absorption of water in concrete[23]. For cementitious materials, these models fail to describe their anomalous behaviour. This is because Richards' equation considers a stationary pore structure[23,24]. Hence, it is necessary to include in the formulation the change in the pore structure during water absorption. For that, a modification to Richards' equation is proposed including a time-dependent permeability[24,25]. This allows to include the changes in the pore structure caused by the sensitivity of C-S-H to water by means of a kinetic parameter.

The major aims of this research are to quantify the moisture-dependent deformations as function of time, and to simultaneously visualise imbibition profiles to connect changes in the pore structure to the relative amount of porosity and deformable phase fractions. Additionally, an inverse analysis is conducted using Richard's equation considering time dependent permeability to link the model parameters to the pore-

structure of the tested materials and to demonstrate such model can correctly capture the observed imbibition behaviour in cementitious materials. The intended outcome is to obtain a complete description of water ingress in cement-based materials by highlighting the idea of a varying pore structure during imbibition. Thus, there is a great need for future models to consider the change in pore structure during water transport.

2. Materials and methods

2.1. Mix composition, samples and preconditioning

Cement pastes were prepared with Portland cement CEM I 52.5 N and white cement (chemical compositions provided in Supplementary Material). Quartz was used in two mixes to replace part of the cement and hence decrease the relative amount of deformable phases (C-S-H). The added quartz had similar particle size distribution to the CEM I (laser diffractometry results in Supplementary materials). This fine quartz was added as an "inert filler" to study the effect of reducing the amount of deformable phases (having less cement) but using a cement replacement with a similar particle size distribution. Quartz replacement level (34 % of the cement, in wt.) was based on the maximum amount of quartz that could be included without significantly affecting the workability of the pastes. Mix composition is given in Table 1. Prismatic samples of 40 mm x 10 mm x 15 mm (length x width x height) were cast, unmoulded after 48 h and cured for 1 year in a conditioned environment at (95 +/- 5) % relative humidity and (20 +/-2) °C. The extended curing period was chosen to reach an almost fully developed hydration degree and ensure minimal interference of further hydration during imbibition.

Table 1. Cement paste mix compositions

Mixes	P4	P6/W6	PQ/WQ
Water (g)	58	87	75
(white) Cement (g)	145	145	125
Quartz (g)	0.0	0.0	42.6

2.2. Characterization of cement pastes

The pore structure of the pastes was assessed by water absorption under vacuum (WA) and mercury intrusion porosimetry (MIP).

For WA, three prismatic samples of each cement paste mix were cut into slices of (10 ± 2) mm and put under vacuum (0.1 bar) for 2 h (n = 9). Water was then drawn into the vacuum chamber until the samples became fully immersed. Vacuum was released and samples were kept under immersion for 24 h. The saturated mass (m_{sat}) and immersed mass (m_{im}) were registered. The dry mass (m_d) was determined afterwards by drying the samples in an oven at 105 °C and until stable mass (dm/dt < 0.1 wt.%/24 h). The value of WA porosity was determined as $(m_{sat} - m_d)/(m_{sat} - m_{im})$.[7]

For MIP, crushed samples of each paste of about 1-2 g were obtained from the core of a prismatic sample (n = 2). The hydration was stopped by solvent exchange with isopropanol following the RILEM recommendations[26]. The maximum pressure applied was limited to 200 MPa to avoid cracking induced by excessive pressure. The surface tension and contact angle adopted were 482 mN/m and 142º, respectively. The theoretical model of cylindrical pores was used to translate the results into pore entry diameter by means of the Lucas-Washburn equation. With the data obtained, the intrudable porosity, entry pore size distribution, tangent and critical pore entry size were calculated.

To quantify the C-S-H content in the cement pastes, XRD coupled with Rietveld + PONKCS[27] was performed, using zincite as internal standard. Specimens hydration was stopped following the RILEM recommendations[26]. Details about sample preparation and apparatus setting are given in the Supplementary Material section.

2.3. Assessment of external deformations during imbibition

The vertical and horizontal external deformations experienced during imbibition were registered by two precision strain gauges attached vertically (V) and horizontally (H) (Figure 1). Strain gauges with linear patterns for use on cementitious surfaces were used, their overall width and height were 6.35 mm × 31.75 mm and 4.57 mm × 8.26 mm, for the horizontal and vertical strain gauges, respectively. The strain gauges were glued with epoxy to the specimens covered with an additional layer of epoxy. Cables were attached with two soldering points. Such cables ended in a connector that was used to easily connect and disconnect the samples to the data acquisition unit before and after weighting. Aluminium tape was used to cover the samples laterally, leaving the top and bottom of the sample uncovered. This allowed one-directional liquid flow and protected the strain gauges connections from direct contact with liquid water. The preconditioning of the specimens consisted of immersing them in water for 72 h and then drying them in an oven at 40 °C until the weight loss was lower than 0.2 % in a 24 h period, which took around 1.5 weeks. After the preconditioning, specimens were kept in double plastic foil and left at 20 °C for around a week to achieve a homogenous moisture distribution.

2.4. Neutron radiography experimental set-up and image analysis

The visualisation of water ingress was achieved by means of neutron radiography experiments at the NEUTRA facility [28], part of the Swiss spallation neutron source SINQ of the Paul Scherrer Institut (PSI) [29]. The neutron beam of the spallation source was guided to a fixed size aperture of 20 mm in diameter by means of a convergent inner collimator tube. From there, a divergent outer collimator led the neutron beam to the object space with a useful rectangular area of 150 mm side. The thermal energy spectrum of the neutron beam was characterised by a Maxwell–Boltzmann distribution with peak energy of 25 meV. The neutron beam then passed through the studied samples to a 30 µm thick Gd_2O_2S:Tb scintillator screen (manufactured in collaboration between RC-Tritec, Teufen Switzerland and PSI). The scintillator converted the neutrons to visible light, which was deflected by a mirror inside the camera box (MIDI-box set-up) and recorded by a CCD (Andor iKon-L) with a 50 mm Zeiss Otus lens. The pixel size of the acquired images was equal to 86.9 µm. A rigid aluminium frame was made ad-hoc to position the trays where specimens would be placed for the imbibition experiment. The trays were also made of aluminium to minimise neutron interaction. The design of such trays was based on a “dam system” with two separate reservoirs: one for the specimens and the other one for liquid overflow. Specimens were placed on 10 mm height supports and a 13 mm division barrier between the reservoirs maintained a constant immersion level of 3 mm (Figure 1). Water was introduced into the trays from outside the bunker with peristaltic pumps. Any additional volume over 3 mm was continuously discharged in the reservoir.

Neutron radiography offers special capabilities to reveal the shape of the wet front as water rises. For this, it is imperative to correctly process the image for an accurate quantification. For this research, the images were processed using Kiptool, a multi-platform general purpose software to process 2D and 3D imaging data[30]. The importance of appropriate data correction for useful results (namely removing sample and set-up scattering by means of black bodies) has been highlighted in previous research [31,32] and was applied here. The steps for image acquisition were as follows: open beam (10 images), dark current (10 images) and black body images (10 images) were obtained for each series to perform the corresponding corrections (neutron beam intensity, camera noise, background scattering). During the

imbibition experiment, 3 pictures per minute were taken. For the image analysis, Kiptool was then used to remove sample and set-up scattering by using black bodies. After that, moisture distribution was calculated from the neutron images using Beer-Lambert's law from the average of 5 pictures per "point" in time (chosen as every 15 minutes).

As a preliminary step, to verify the potential interaction between instrumental systems, twin samples were tested inside and outside the bunker with the following purposes: (1) determining if neutrons could interact with strain gauges and interfere in the deformation measurements, and (2) verifying that twin samples outside the bunker without strain gauges would provide similar water ingress results as the one inside with strain gauges. The results were equivalent showing no significant effect of the neutrons on the strain recording. Additionally, samples without strain gauges were measured in the bunker to check the effect of the strain gauges on the neutron images (and hence on the following water content determination). The presence of strain gauges did not disturb the water content analysis from neutron radiography neither the deformation measurements.

To evaluate the whole primary imbibition period, the whole imbibition experiment lasted for at least 24 h. First, samples were exposed to neutrons in the aluminium frame and kept in contact with water for 5 h. After that, samples were weighed and placed again in contact with water in another tray but no longer exposed to neutrons. The last gravimetric measurement of mass gain was about 24 h after first contact with water. All imbibition experiments (inside and outside the bunker) were conducted at around 25 °C.

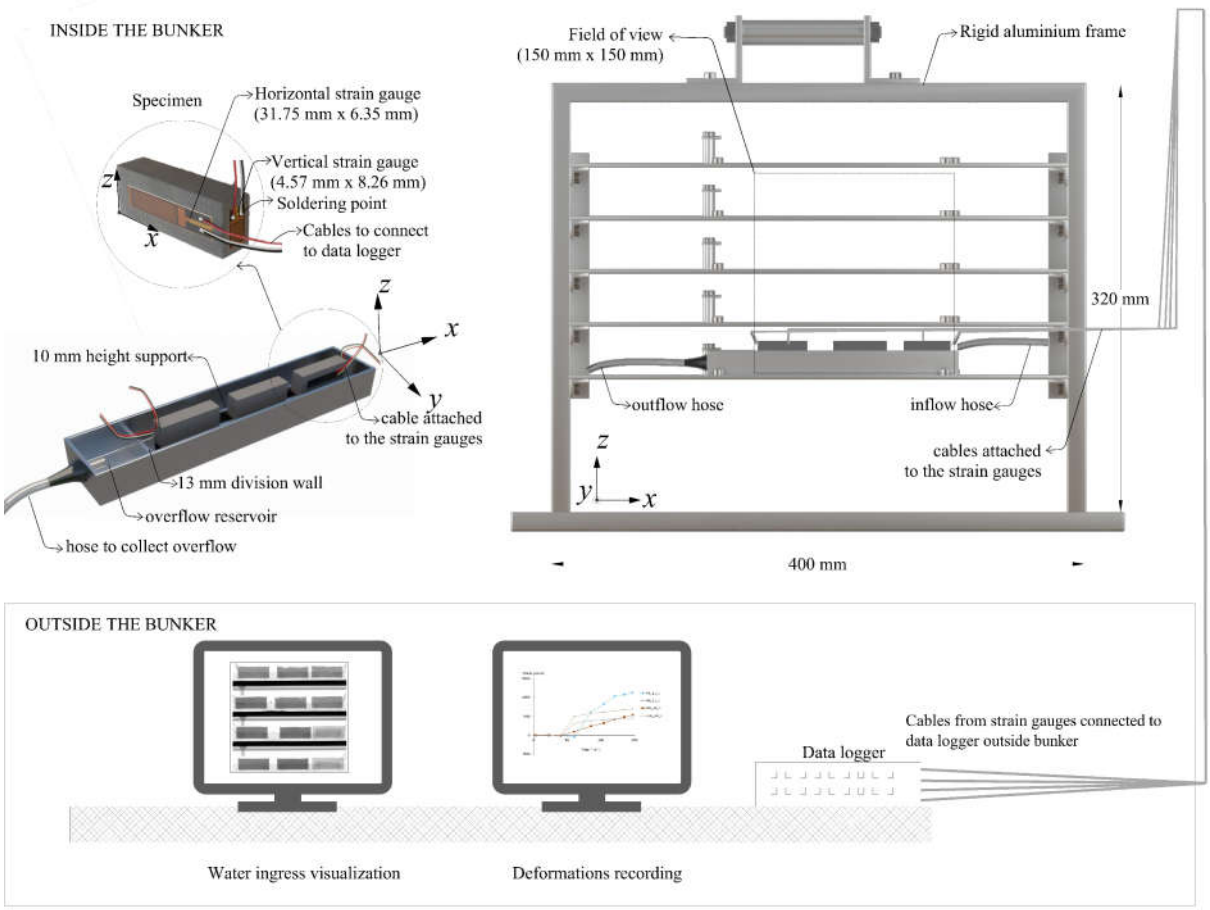

Figure 1: Neutron-imbibition-deformation set-up of cement paste samples, inside and outside the bunker for continuous deformations and water ingress assessment.

3. Results and Discussion

In this section, the influence of porosity and pore size distribution on imbibition is discussed (3.1), and results of porosity and C-S-H content are linked to the obtained deformations (3.2) to evaluate the influence of these parameters on the strains. Following that, the water content computed from image analysis of the neutron radiographs is compared to gravimetric measurements (3.3) and the calculated water content profiles are discussed (3.4). Finally, the influence of water availability on the deformations of the samples is evaluated (3.5).

3.1. Porosity, pore size distribution and capillary imbibition

Undoubtedly there is a strong link between the pore size distribution of a porous solid and capillary imbibition. For this research, MIP and WA were used to characterise the microstructure of the pastes.

WA allows to determine total porosity, as water is forced into the whole pore structure and mass is measured in a complete saturated sample. Although water is involved in the measurement, there is no swelling effect of C-S-H on the WA results because it happens at expense of water entering the interlayer space, so the pore volume filled with water is the same. Results from nuclear magnetic resonance evidenced the immediate effect of water invading empty pores and a second invasion of gel pores causing swelling[33,34]. When measuring porosity with WA, the whole volume of the sample changes when internal swelling occurs.

There is some debate about the drawbacks of MIP as a technique to describe the pore structure of cementitious materials. One of the main limitations is that, for reliable results, measurements are made in vacuum dried samples given that MIP results are very sensitive to the moisture content in the samples. Hence, the pore structure during imbibition is not exactly the same as reflected by MIP. This and other points are discussed in the interesting review made by Diamond[35], who still acknowledged the usefulness of determining the intrudable pore volume and characteristic diameters. Hence, for this research intrudable porosity and critical and tangent pore entry size are derived from the MIP data. The critical and tangent entry pore sizes were calculated as indicated in previous research[36].

Figure 2 (a) shows the differential curves measured with MIP of all studied mixes. Clearly, P4 is the mix with the lowest intrudable pore volume and WQ the mix with the largest intrudable pore volume. However useful measuring the initial pore structure is, caution should be taken when modelling as to consider it stationary during water ingress. The water transport is influenced by the restriction of the mix which in turn affects the internal dynamic porosity.

Figure 2 (b) displays the primary imbibition capacity (defined as the amount of water in the sample after 5 h of imbibition per exposed area), the total pore volume (obtained from MIP and WA) and intrudable capillary pore sizes obtained from MIP. Note that the comparison is made considering the capillary imbibition capacity and not the capillary imbibition rate (transport rate). This is because porosity (absorption capacity or water intrudable volume) is more comparable to the capillary imbibition capacity, as in both cases volumes are being analysed. The considered capillary pore ranges are 0.01 - 0.1 μm (as proposed by Mehta and Monteiro[37]) and 0.01 - 0.05 μm (as proposed by Mindness[38]). Measuring total porosity with WA provides information about the water accessible porosity, while MIP gives information about mercury accessible porosity. This difference leads inevitably to higher values of porosity with WA in comparison to MIP. When comparing total porosity to imbibition capacity, the linear correlation is not optimal:$R^2 = 0.75$ for MIP and $R^2 = 0.56$ for WA. This is explained by the lack of sensitiveness of C-S-H to mercury and indicates that pore structure does not remain the same during imbibition. As mercury intrudes the sample, there is no swelling. Therefore, the lack of correlation can be connected to the missing consideration of the C-S-H phase content in the samples. The poor

correlation between these porosity parameters highlights how initial static pore size cannot be the only factor affecting capillary water transport.

Wang et al.[39] investigated the relation between porosity (measured by MIP) and capillary absorption coefficient (calculated with the traditional square-root of time approach) in different concrete mixes. They found a bilinear trend where 12.87 % is a critical porosity value for concrete, for lower values, no rapid increase of sorptivity was found. However, when porosity was larger than that critical value, the capillary water absorption coefficient increased rapidly as the porosity increased. Such critical value or bilinear trend is not observed in the tested cement pastes. Results obtained from WA and MIP (Figure 2 (b)) display a general increasing trend (coarser pore structure leading to higher imbibition capacity) for the very varied group of cement pastes. Although MIP results have a better correlation with imbibition capacity (probably because only a certain range of pores can be assessed with MIP), it seems that another factor plays a role during water uptake. This points out that during the dynamic process of imbibition, pore structure cannot be considered static, as it can for WA (saturated sample) or MIP (dry sample).. Results from MIP can be considered as descriptors of the initial pore structure and WA represents the porosity of a saturated sample. In this sense, shifts in both critical and tangent pore entry size with the relative humidity has been reported[40,41], hence the same would apply during capillary imbibition.

Figure 2 (c) shows the critical and tangent pore entry size and the primary imbibition rates of all mixes. While the tangent pore entry size follows at least partially the same trend as the primary imbibition rate, the critical entry pore size is apparently not linked with imbibition. The tangent entry pore size represents the first percolation process and hence it is much more linked to the speed of water ingress. The critical entry pore diameter on the other hand, is more related to diffusion processes, as it is usually within the gel pore range (< 0.05 µm)[42].

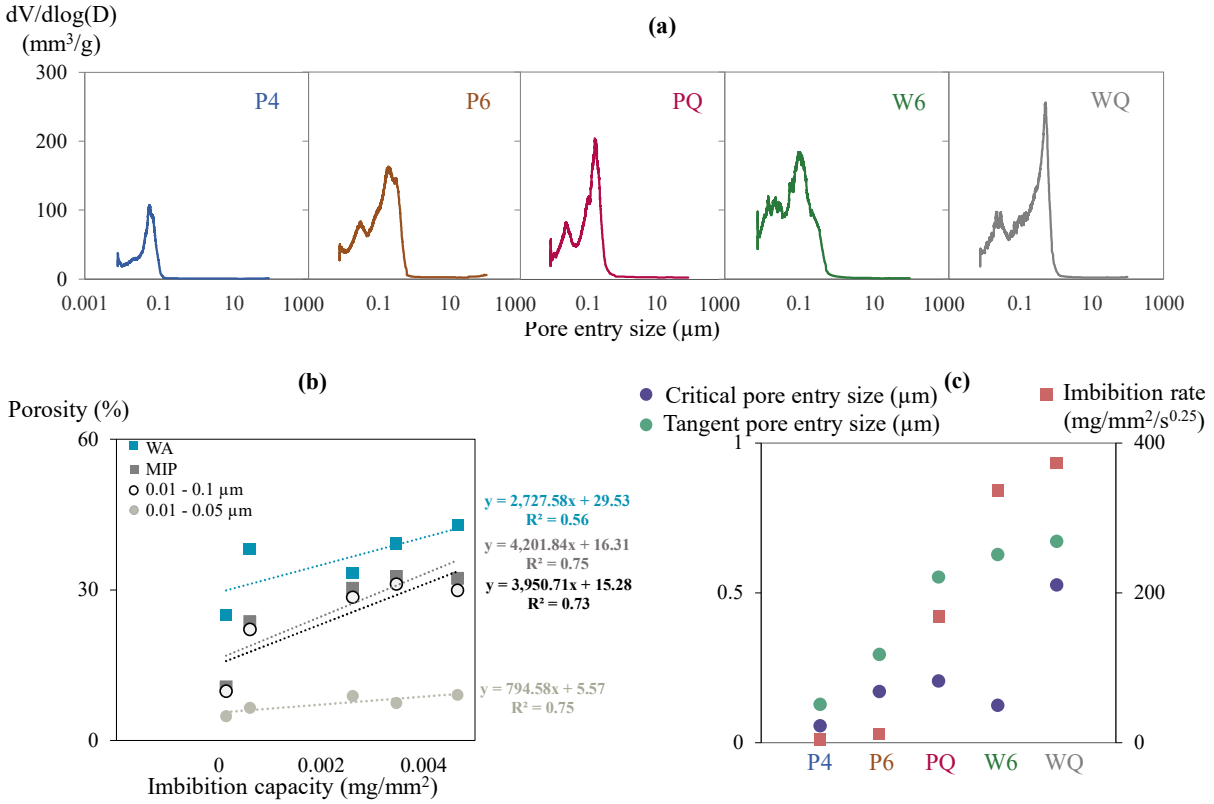

Figure 2: (a) differential curves obtained from MIP; (b) relation between porosity (from MIP and WA) and imbibition capacity; (c) relation between critical and tangent entry pore size and imbibition rate.

3.2. Mix composition and deformations

The role of the mix composition was analysed by contrasting the deformations with the porosity and C-S-H content. A visual representation of the measured deformations, the capillary imbibition set-up and of the conceptual view of the paste phases (not to scale) is given in Figure 3 (a). The external deformations were measured with horizontally and vertically placed strain gauges (perpendicular and parallel to the direction of the water flow, respectively). The schematic representation of the cross-sectional view of a cement paste shows how the matrix can be divided into three components: porosity, deformable phase (C-S-H) and non-deformable phase (rest of the paste). These three components were quantified and their relation to deformations was analysed.

Results in Figure 3 (b) correspond to the quantification of the deformable phase C-S-H (obtained from XRD+Rietveld) and the quantification of the porosity (obtained from WA) contrasted with the volume increase quantified from the horizontal and vertical deformations measured at 5 h of imbibition. As the measurement direction has an impact on the values [8], the volume increase was calculated to consider both directions in a proportional way in relation to the sample geometry. The "deformed" volume of the sample was calculated and compared to the original. The difference in volume is presented as the "volume increase" in percentage. Blue rounded markers show porosity values versus volume increase, green rhomboidal markers show C-S-H content versus volume increase. If the material would only be composed by a deformable phase and porosity: higher porosity would lead to lower external volume increase (because it can deform internally), and higher amount of C-S-H would lead to higher volume increase. Results indicate that neither porosity nor C-S-H relate with all deformations in a consistent way. Hence, it is not possible to conclude that an increasing amount of C-S-H content directly leads to overall larger external deformations, or vice versa. Similarly, an increasing amount of porosity does not always lead to lower volume increase. The lack of agreement with the expected trends considering only C-S-H and porosity highlights the influence of the restriction in the external deformations.

The most adequate option seems to analyse the impact of the relative contents of the three phases, in order to analyse the mix composition as a whole. This can be done with the model of Thomas and Jennings[43] that considers the relative amount of porosity, deformable and non-deformable phases, and their influence on the restriction of the system. Additionally, the model allows determination of a singular limit value of deformations for the case when porosity does not change. This is of particular interest because based only on the values of the external deformations, we cannot assume if the pores shrink or swell. Hence, to study the influence of the relative amount of the three phases on the deformations suffered by a porous solid, the relation between the final volume and initial volume ($V_f/V_i = k_{tot}$) was calculated as given by Equation 1[43] in Figure 3 (c). Re-arranging the expression and considering no change in porosity (final volume of porosity/initial volume of porosity = $k_p = 1$) Equation 2 is obtained. This equation indicates the limit deformation that the deformable phase should suffer (k_{deflim}) so that the porosity remains the same (given a certain external deformation k_{tot}). If it deforms more, pores shrink; if it deforms less, pores expand. One can already see that, when there are deformations, the case that porosity does not change is an exceptional one. Hence in presence of deformations, is much more likely that porosity changes.

Based on the experimental data (Figure 3 (d)), the calculated values of k_{deflim} (rounded purple markers) so that porosity does not change are plotted together with the volume increase (orange rhomboidal markers). Results show a good relation between volume increase and k_{deflim}. This highlights the need to take both C-S-H and porosity in a combined manner (included in the k_{deflim} parameter) to describe their effect on the deformations of the paste. Note the contrast between the trends found in Figure 3(b) – considering the isolated influence of C-S-H and porosity- and Figure 3 (d) – considering k_{deflim} that combines both C-S-H and porosity in one parameter.

Another point to highlight is that for all mixes, the value of k_{deflim} is lower than 1.006. This means that, should C-S-H deform more than 0.6 % (which most likely happens[44]), then pores would shrink.

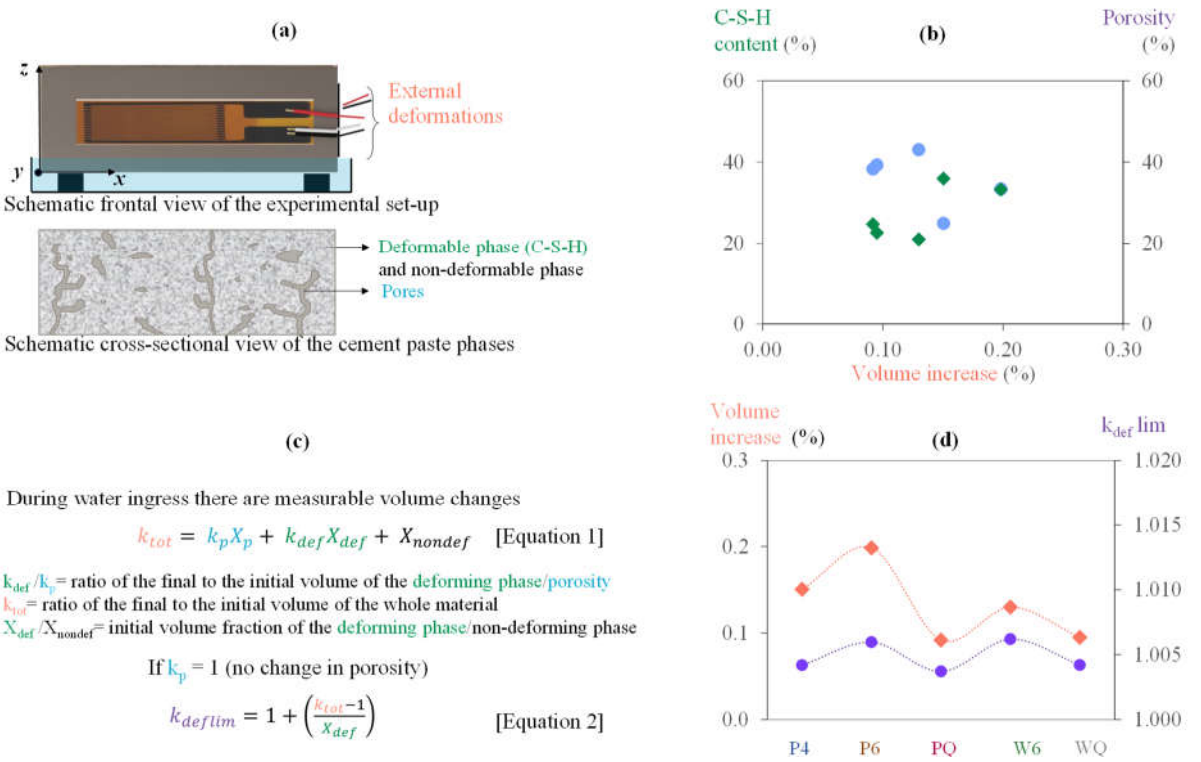

Figure 3: (a) Visual representation of set-up and conceptual representation of deformations, porosity and C-S-H (not to scale); (b) experimental results of C-S-H content (green rhomboidal markers) and porosity (rounded blue markers) as function of volume increase; (c) theoretical relation between the three parameters; (d) values of the limit value of K_{deflim} in relation to the volume increase.

Overall, results show that deformations occur in cementitious materials, with different w/c and binder types. Specifically, the k_{deflim} threshold value after 5 h of imbibition described the maximum deformation that C-S-H could experience without changing the pore size. This limit value obtained is very small for all mixes in comparison to the deformation that C-S-H would experience inside the cementitious matrix[44]. According to the model, this indicates that pores necessarily shrink during imbibition. Still, bulk deformation is a result of competing C-S-H swelling and the restriction provided by the rigid phases. Due to the heterogeneous nature of cementitious materials, this competition is highly unbalanced.

The complex porosity of a cementitious matrix as described by Bede et al.[45], is in absolute contrast with the usual cylindrical pore model still very much used to interpret imbibition results. The structure depicted is in alignment with the NMR results[6,12,14] that invoke swelling of C-S-H leading to less volumes of gel pores. This structure also aligns with the restriction concept discussed above. The restriction provided by the non-deformable phase leads C-S-H sheets to deform mainly towards the capillary pores. The case of a more porous matrix for a given C-S-H content results in more deformations towards the inner porosity than externally. This could be an explanation for the largest deformations experienced by P4, which is more restricted to freely deform internally (because of the low porosity and high C-S-H content), so that more deformations are detected externally.

3.3. Gravimetric results versus neutron radiography results

To verify the water content calculations, a region of interest (ROI) was defined in the middle of the sample to determine the water content during the imbibition experiment. This ROI was chosen as large as possible, while avoiding the boundaries of the samples (to reduce possible edge effects) and avoiding

the submerged part (where it is not possible to calculate water content due to the too large attenuation of the beam in the water pond). The water content from the ROI at the end of the experiment was then extrapolated to the whole area of the sample and compared to the gravimetric results obtained from weighing the sample directly after the beam exposure. Results shown in Figure 4 indicate that water content calculated from the ROI is fairly similar as the one determined gravimetrically. The overall trend is slightly lower for the neutron-based values than for values obtained from the gravimetric measurements. This is because the part of the sample that was immersed has probably a slightly larger water content than the rest of the sample. Still, the comparison shown in Figure 4 validates the water content calculation obtained from the neutron radiography image analysis.

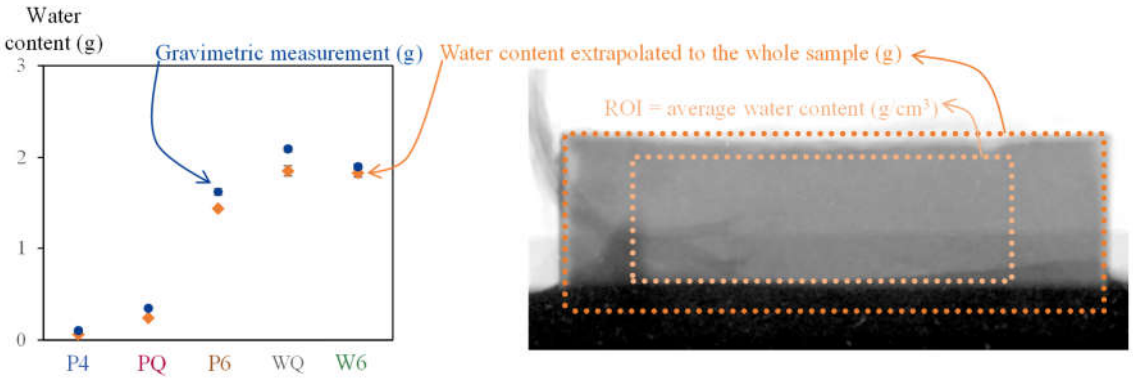

Figure 4. Comparison between average gravimetric and average image based water content for each mix.

3.4. Shape of the water front and quantitative water content by neutron radiography.

Calculations made from the neutron radiographs allowed to determine the spatial and temporal evolution of water content and local saturation degree $0 \leq f(z, x, t) \leq 1$. At least 3 samples per mix were evaluated in the neutron radiographs. Figure 5 shows in each case the mean value ($n \geq 3$) of samples from the same mix with the corresponding standard deviation. The water content along x it is determined and then averaged, this average variation with z as a function of time is represented in the curves from Figure 5 (a). Hence, each curve represents the lateral average (that is, the vertical concentration profile $\bar{f}(z, t)$) of the water content measured every 15 minutes. The integral of the curves represents the water content in the sample at that time. Such mass gain, quantified with image analysis of the neutron radiographs, is displayed in Figure 5 (b) as a function of the fourth root of time.

One of the most interesting results is the variation found in the shape of the water profile for different mixes. Figure 5 (a) displays the water profiles of the studied mixes, where the water profile does not develop as a sharp penetration front advancing over height. The unusual shape of PQ and WQ is due to a larger initial immersion depth on those samples (samples from both mixes were in the same tray). So the water content on the bottom was much affected by the water level. As time progressed, the water content on the bottom decreases because the water level decreased and adopted and stable value (3 ± 1 mm). It is possible that part of the lack of sharpness in water penetration is due to the thickness of the samples, as the profiles are the average of the grey values over the thickness. Hence, some deviation from a penetration front evolving parallel to the base of the samples over time could be expected. However, considering similar variabilities over z and x of the water content for a certain height, the lack of sharpness cannot be fully explained by the thickness of the samples. The deviation from a sharp water penetration front can partially be due to water penetrating at different rates over a wide range of pore sizes, which are under dynamic changes as water ingresses in the sample. Some authors offer demonstrations of how pore shape influences the liquid flow[46], and how shape variations modify the water flow[47]. The multiscale pore structure of cement paste (described in Figure 2 (a)), gives rise to

complex water distributions, explaining the lack of a sharp water front. Similarly, Hallaji et al.[48] studied water ingress in cement pastes (w/c = 0.6, age = 22 days) with neutron radiography and found lack of uniformity and even some lack of symmetry of the flow, which they attributed to porosity gradients within the samples. Nonetheless, a comprehensive description of imbibition includes a more complex process involving C-S-H swelling and water binding. The particularity with water is that not only water is bound by C-S-H, also changes in pore structure occur. The highly heterogeneous solid structure of cementitious materials and the changes in the pore structure challenges the applicability of classical approaches of water uptake and reveals the need to examine water imbibition description considering a dynamic porosity.

In Figure 5 (b), the rounded markers represent the mass content every 15 minutes. The slope of the linear fitting is indicated in each graph. The studied range of internal restrictions, porosities and deformations did not affect the correlation with the fourth root of time to a significant degree. This indicates, as seen in other research[49–51], the validity of such approach for describing capillary ingress in a wide range of types of cementitious materials. During the first 5 h of imbibition, the primary imbibition rate was calculated as a function of the fourth root of time. As expected, the mix with lowest porosity (P4), leads to the lowest imbibition rate whereas the mix with the largest porosity has the largest imbibition rate (WQ). Additionally, WQ reached a change in slope to a much lower water ingress rate even before the 5 h. Probably the fast water ingress rate of WQ led to a quick saturation by capillarity and hence the secondary imbibition period started sooner. That is way, in the mass gain figure of WQ there are two equations that indicate the primary and the secondary imbibition rate. After removing the samples from the neutron beam exposure at 5 h of imbibition, samples were weighed and kept in contact with water for a total period of 24 h. The gravimetric measurements of the samples after 5 h and 24 h of continuous imbibition are indicated with rhomboidal markers. Mind the excellent match between the neutron radiography determined water ingress (circle markers) and the one determined gravimetrically (rhomboid markers), as previously discussed in section 3.3.

The slower water ingress when capillary forces stop being dominant is called secondary imbibition[51,52]. The secondary imbibition period for the tested paste samples starts after 5 h of imbibition. Based on the neutron radiography images, we observed that water had reached the top of the samples and hence the main driving force stopped being capillarity. However, gravimetric measurements after 5 h and 24 h are insufficient to determine the secondary imbibition rate. More points would be desirable to confidently describe the secondary imbibition slope.

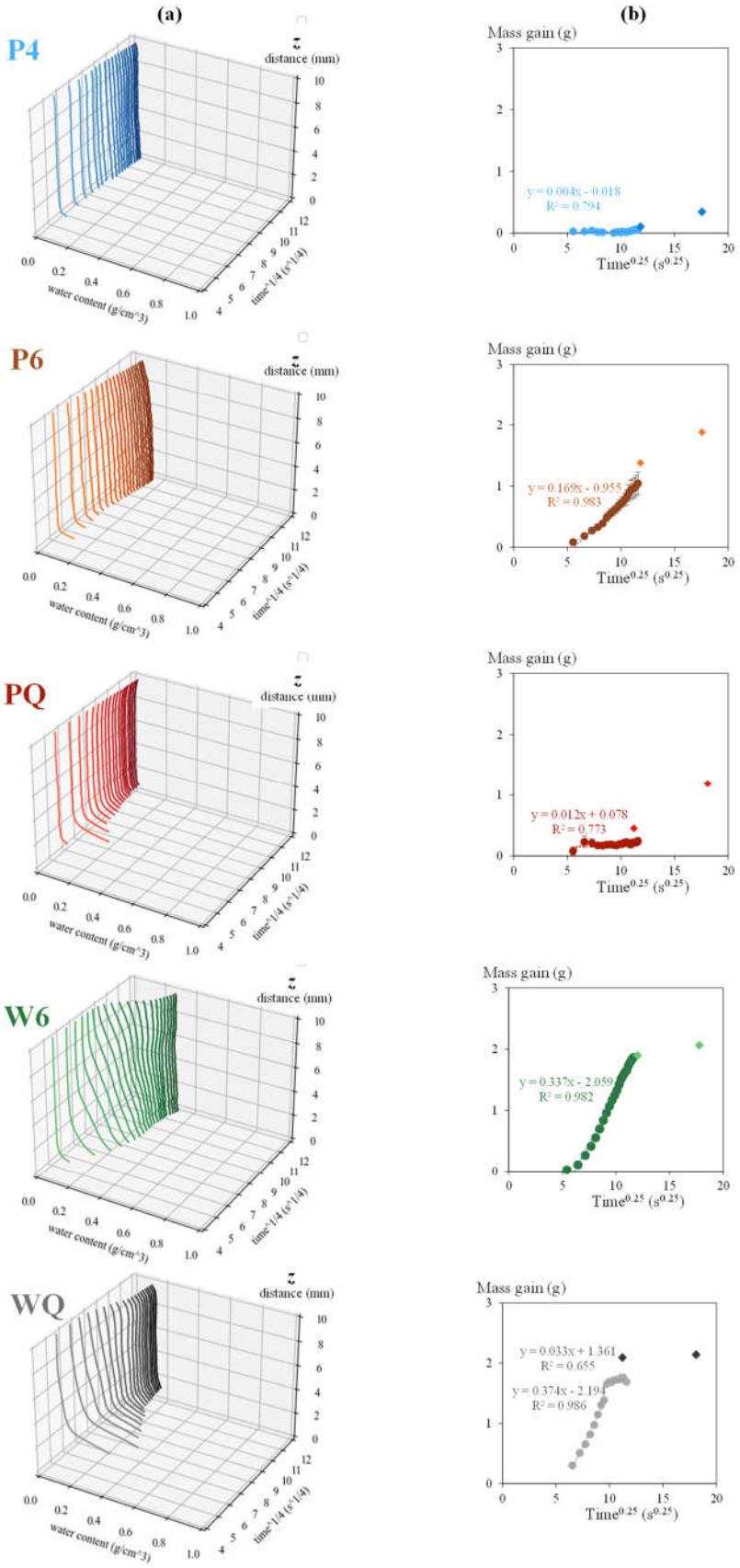

Figure 5. Spatial and temporal evolution of water content and mass gain evaluated from neutron radiographs: (a) spatial and temporal evolution of the vertical profile from neutron radiographs; (b) evolution of mass gain calculated from neutron radiographs (rounded markers), evolution of mass gain from gravimetric measurements (rhomboidal markers).

3.5. Water availability and deformations

It seems straightforward that more water uptake would lead to larger external deformations. This would be the case if no internal restrictions were present. There certainly are internal restrictions and, notably, the relationship between water uptake and external deformations is not unique for all the samples. In fact, P4 had the lowest water uptake and relatively high strain values, whereas WQ had the highest water uptake and relatively low deformations (Figure 3). Therefore, deformations may be less related to mass gain but rather to water availability inside the pore structure. To visualise this, the water content was calculated and then transformed into saturation degree considering the porosity of each mix and the initial water content. The region where the water content was determined corresponds to the area covered by the horizontal strain gauge. This was done to evaluate if there is a direct relation between water availability in a certain zone and the deformations measured in the same zone.

Figure 6 displays the vertical and horizontal deformations together with the variation of the saturation degree. Although water availability inside the pore structure does not relate in a proportional manner with the deformations, the increasing trend in saturation degree corresponds with the development of horizontal deformations. Still, the scale is not the same for all mix compositions. To achieve similar horizontal deformations, mixes with less C-S-H content (W6, WQ) reached higher saturation level than mixes with more C-S-H content (P4, P6. PQ). Again, the multifactor justification evidences that an increase in water content is not reflected in comparable deformation increase when analysing different mixes. For example, in the case of vertical deformations, results in Figure 7 show P4 and P6 having the highest vertical deformations but not the highest saturation degree. Whereas WQ and W6 have the highest saturation degree and the lowest vertical deformations. Huang. et al.[53] studied the linear deformation of cement pastes with different w/c and they found that the cement paste with the lowest w/c produced higher swelling. Results shown in Figure 7 follow a similar trend, with P4 having the lowest w/c and highest vertical deformations, and W6 and WQ with the largest w/c showing the lowest vertical deformations. However, measurements from vertical deformations do not follow the saturation degree trend at the position of the strain gauge. This is because vertical strain gauges measure changes along the whole height of the sample and hence saturation degree is variable. Additionally, vertical deformations are negative at the beginning because of their position in relation to the water flow, as discussed in previous research[7,54]. To summarize, the saturation degree alone is not enough to explain the deformations. As discussed above, restrictions and C-S-H influence the deformations and the water flow.

External deformation measurements indicate that the total volume of the sample slightly increases. However, changes in the total pore volume are not substantial. During imbibition, C-S-H necessary swells, and the most relevant consequence of this swelling is the dynamic change caused in the pore sizes during water ingress and hence dynamic change in the flow path. There is an internal dynamic porosity that is influenced by the restriction of the mix and that influences the water transport. This dynamic porosity was also observed in recent research[55], where cement pastes with an ultra-low w/c (0.17) were evaluated under different curing conditions to determine the evolution of pore size changes caused by water movement. NMR results showed the swelling of C-S-H contributes to the increase of gel pore volume[55]. Overall, deformations highlight the relevance of considering a dynamic pore structure during the transport process in new models. This is accounted in our proposed model through time dependent change in permeability once water is in contact with the sample.

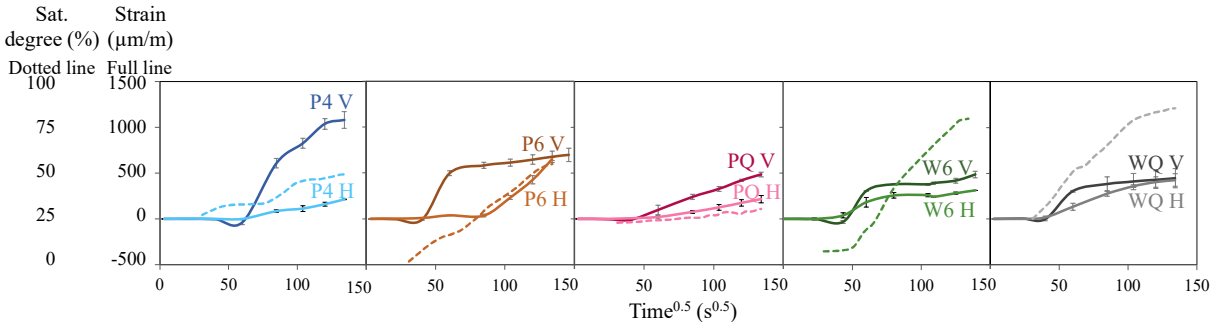

Figure 6. Strain and saturation degree variation as a function of time$^{0.5}$. Full lines: vertical (V) and horizontal (H) deformations. Dotted lines: saturation degree at the position of the horizontal strain gauge.

4. Proposed modelling approach

The aim of the numerical model proposed consists in considering the anomalous behaviour of cementitious materials in moisture transport processes. The physical swelling of C-S-H sheets along with the consequent dynamic pore structure lead to time-dependent water transport properties. So, changes in pore structure caused by the sensitivity of C-S-H to water are included in our model by means of considering the variation of permeability values with time[25,56].

The transport process of water in a porous media under the assumption of constant gas pressure can be modelled through Richards transport equation, which is written in terms of capillary pressure (P_c), Equation 3:

$$\left[\varphi \frac{\partial S_w}{\partial P_c}\right] \frac{\partial P_c}{\partial t} = \nabla.\left[\frac{K_w(s_w)}{\mu_w} \nabla P_c\right] \qquad \text{[Equation 3]}$$

where φ is porosity, S_w, is degree of saturation, P_c is capillary pressure, μ_w is dynamic viscosity, and $\frac{\partial S_w}{\partial P_c}$ is called water retentions capacity which can be determined through constitutive relationship between S_w and P_c. Van Genuchten model was adopted to determine the degree of saturation as a function of capillary pressure, Equation 4:

$$s_w = \left[1 + \left(\frac{P_c}{P_g}\right)^{n_g}\right]^{-m_g} ; \text{with } n_g = \frac{1}{1-m_g} \qquad \text{[Equation 4]}$$

P_g is the pressure scaling parameter and the relationship between m_g and n_g is indicated in Equation 4. Permeability is calculated as a funtion of saturation degree and time, Equation 5:

$$K(s_w, t_c) = K_{sat} * K_r(s_w) * K_t(x, t_c) \qquad \text{[Equation 5]}$$

Where K_{sat} is saturation permeability, K_r is relative permeability and K_t is time dependent permeability. K_r is obtained using the Maulen model. By introducing van Genuchten capillary function in Maulen model, Equation 6 is obtained:

$$K_r(s_w) = s_w^k \left[1 - \left(1 - s_w^{1/m_g}\right)^{m_g}\right]^2 \qquad \text{[Equation 6]}$$

where k is a parameter that considers tortuosity.

Finally, to include the variation of permeability with time (K_t), the expression proposed by Hall[25] was implemented, which accounts for change in permeability once water is in contact with the sample, Equation 7:

$$K_t(t_c) = K_1 + (K_0 - K_1) * \exp\left[-\frac{t_c(x,t)}{\tau}\right]^{\alpha} \qquad \text{[Equation 7]}$$

where K_0 is a factor representative of initial permeability, K_1 is a factor representative of long term permeability, τ is a time constant, α is the stretching exponent, always positive, and t_c is the contact time[25]. In this model, K_0 was considered equal to 1 and K_1 as $1/10*K_0$. Contact time is the duration of direct contact between water and matrix. For that reason, t_c depends on the position of the water front (x) at time t.

The model was implemented in a Python code using Fipy[57] using a finite volume solver for partial differential equation. To determine Van Genutchen model, model parameters of time dependent permeability and K_{sat} inverse analysis was used. To ensure global minima differential evolution[58] available in Scipy, was used for inverse analysis process. The objective function was squares of residue obtained by comparing the mass gain results obtained from the model with the neutron experiments. For all mixes, K_{sat}, τ, α, m_g and P_g were determined through inverse analysis are summarized in Table 2. The objective of implementing Hall and van Genuchten models together to calculate permeability values is to describe the anomalous moisture transport behaviour of cement pastes through a kinetic variable, which depends on contact time (Hall model) and degree of saturation (van Genuchten model). This concept is in line the time-dependent transport coefficient for modelling moisture transport described by Zhang and Angst[56] using dual porosity approach. However, they describe the moisture transport divided in large and small pore regions, with different permeability values each. Such an approach would require more parameters to be inferred from inversed analysis and hence avoided in this study.

In Table 2, the parameters obtained from the optimisation process are shown. As it was expected, mixes with higher values of w/c ratio present higher values of K_{sat}. The mix with the lowest w/c ratio and porosity (P4) presents the lowest values of Hall model parameters (τ and α). Also, comparing P4 with P6, both mixes with Portland cement, the values of τ and α for the second are considerably higher than for the first. τ and α control the rate at which permeability decreases with time, the reason for higher values for P6 than P4 can be related with the higher values of porosity for P6.

Comparing both mixes with quartz, but with different types of cements, Portland (PQ) and white (WQ), the last presents higher values of α than PQ. This behaviour can be related with the higher value of porosity presented by WQ.

Table 2. Parameters obtained from model optimisation

Mix	Parameters				
	m_g	P_g	K_{satp}	τ	α
	(-)	(MPa)	(m/seg)	(days)	(-)
P4	0.381	21.64	$4.13\ e^{-15}$	0.32	0.013
P6	0.449	23.60	$4.24\ e^{-14}$	1109.41	1.448
W6	0.483	5.50	$5.37e^{-14}$	808.32	0.208
PQ	0.568	37.02	$6.35\ e^{-14}$	577.70	0.166
WQ	0.494	8.00	$5.00\ e^{-14}$	73.21	0.297

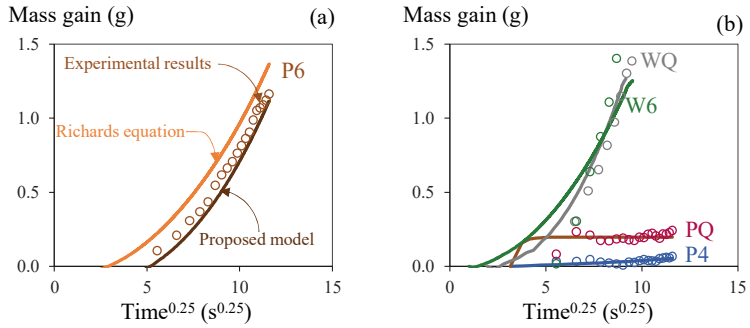

Figure 7. (a) Adjustment of P6 experimental data to Richards model and our approach :Richards with time variation permeability (proposed model). (b) Model adjustment with experimental data

Figure 8 (a) presents the comparison between experimental results of mass gain against the fourth root of time of P6 (experimental), results obtained from Richards equation, and considering time variation permeability (proposed model). The results obtained combining Richards equation with Hall model show a better adjustment with experimental results than those obtained just using Richards equation with non-time dependent permeability. From the experimental results shown from P6, we see how our proposed model describes better the process. This means that it is fundamental to consider the variation of transport properties with time to obtain a realistic modelling of experimental data.

Figure 7 (b) displays the comparison between the experimental results during the primary imbibition period from the rest of the mixes and the modelling results with our approach. The results obtained confirm the model can capture mass gain in these mixes, considering indirectly the change in porous structure in cement mixes through time-variation permeability.

5. Revising how water uptake in cementitious materials is envisaged: an analysis of imbibition in cement pastes

The presented study provides valuable insights into the water dynamics of cement paste, using specifically chosen techniques such as neutron radiography and precision strain gauges. The use of neutron radiographs is highlighted as a non-destructive technique to determine the spatial and temporal evolution of water content and local saturation degree. The lack of a sharp water front visualised through neutron images is linked to the multiscale pore structure of cement pastes combined with a dynamic porosity that influences the water flow. These give rise to complex water distributions. Strain results show that the horizontal and vertical deformations are influenced by different factors, such as porosity and C-S-H content in a combined manner. No dominant relation with either parameter was found. Moreover, it was found that the horizontal and vertical deformations have different responses to saturation degree. Globally, the information gathered here highlights the need of models that describe a variable inner pore structure, which should be included to accurately describe imbibition in cementitious materials. In that sense, the presented modelling approach - although preliminary as further validation on mortar and concrete will be needed - includes several essential concepts that can be used to assess imbibition.

Further research should account for additional factors that may affect the deformations, such as temperature, variable phase assemblage of hydrates, physic-chemistry of C-S-H (e. g., effects of carbonation, pozzolanic action, hydration history).

Capillary imbibition in cement paste is a very complex topic. The remaining limitations faced when performing experiments (as there are assumptions to be made in every experimental technique) still impede to fully describe the link between changes in C-S-H and macroscopic deformations. Most of all due to the inability to assess the actual swelling degree of C-S-H in the cement paste microstructure. The suggested modelling approach still requires further consideration of the highly heterogeneous nature of cement paste. Most certain is that the implications and applications of the findings call for an immediate abandonment of the traditional approach of a rigid pore structure used to describe capillary imbibition in cementitious materials. This is not a trivial task, particularly considering the highly heterogeneous pore structure and the need to fully describe the particularities (anomaly) of the process in cement-based materials.

6. Conclusions

In this research, we have analysed water ingress into cement paste samples via neutron radiography with simultaneous deformation measurements. Conclusions can be summarised as follows:

- Porosity and C-S-H content are not isolated factors affecting external deformations. Hence, it is not possible to conclude that an increasing amount of C-S-H directly leads to overall larger external deformations, or vice versa. Instead, the whole restriction of the system influences deformations.
- External deformation measurements indicate that total volume increases (though slightly). However, changes in the total pore volume are not directly connected to the external deformations. C-S-H swelling develops internally to a certain extent. The change caused in the pore sizes and hence in the flow path is the most relevant consequence of such swelling.
- Results about the deformations occurring during water ingress are solid and urge researchers to describe water imbibition considering a dynamic porosity.
- Neutron radiography allowed to determine how deformations vary similarly with the saturation degree but differently depending on the porosity and C-S-H content of the paste.
- A lack of a sharp water front was visualised with neutron radiography. Changes on the saturation degree obtained from neutron radiographs highlight that deformations are not directly related to water availability when comparing different mixes.
- The presented modelling approach includes the concept of dynamic porosity during water ingress and it adjusts well to the imbibition results of several paste mixes. This will be further extended to have a poromechanical model which also captures the measured deformations.

Acknowledgments

Natalia Alderete (Postdoctoral Fellow, 12ZG820N) and Philip Van den Heede (G062720N) acknowledge the financial support of the Research Foundation—Flanders (FWO).

Yasmina Shields acknowledges the support from the SMARTINCS project; this project has received funding from the European Union's Horizon 2020 research and innovation programme under the Marie Sklodowska-Curie grant agreement No. 860006.

Supplementary material

S.M.1. Chemical composition of used cements

The Table S.1 below shows the chemical composition of the used cements.

Table S. 1. Chemical composition of the used cements.

	Portland cement, CEM I 52.5 N (Wt.%)	White cement, CEM II 42.5 N (Wt.%)
CaO	63.75	66.1
SiO_2	18.14	21.9
Al_2O_3	5.28	2.5
Fe_2O_3	4.18	0.2
SO_3	3.18	2.4
CO_2	1.85	nd
MgO	1.1	0.4
K_2O	0.39	0.35
Na_2O	0.42	0.35
TiO_2	0.34	0.34
Mn_2O_3	0.1	0.1
Insoluble residue	0.74	nd
Loss on ignition	2.48	4.9

nd = not determined

S.M.2. Particle size distribution

Figure S.M.1 shows the particle size distribution of the used CEM I and quartz. The results were obtained from laser diffractometry (Malvern Masterizer 2000), using isopropanol as dispersant. Results are shown to indicate the fineness of the quartz, that was added as an inert filler.

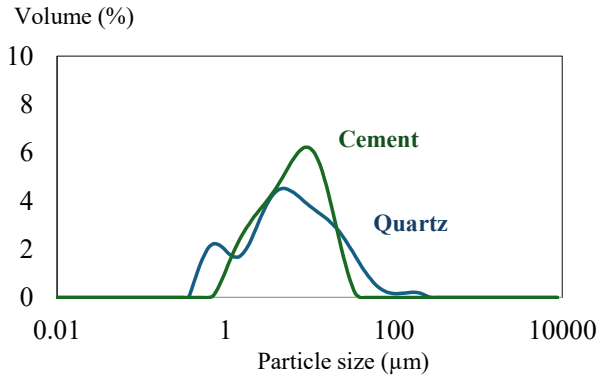

Figure S.M.1. Results of laser diffractometry of the used CEM I and quartz.

S.2. XRD parameters

A prismatic specimen per mix was crushed with a hammer and the interior freshly crushed pieces were collected. Such particles were then ground with mortar and pestle to pass a 1 mm sieve. The whole crushing and sieving procedure was performed as fast as possible (< 10 min) to minimize the exposure to air of the sample. Immediately after, the obtained particles were immersed in isopropanol. The suspension was filtered using a Buchner filter and flask (filter paper with pore size smaller than 2 µm). The filter paper was placed on a watch glass and dried for 8 min in a ventilated oven at 40 °C. After that, the powder was ground, homogeneously mixed with 10 % zincite. For the XRD measurements, side loading was chosen to prevent preferential orientation of some phases. All samples were tested within 48 h after hydration stoppage. Afterwards, all samples were further ground to particle size < 63 µm while blended with 10 % ZnO as internal standard. To prevent preferential orientation of crystals side loading was used for compaction. XRD measurements were taken using CuKα radiation on a Thermo Scientific ARL X'tra diffractometer + Peltier cooled detector operated at 30 mA and 40 kV. Measurements were made at room temperature in step-scan mode (0.02°/seg), scanning the 2θ angle from 5° to 70° to carry out quantitative analyses of the unhydrated cement and pastes.

S.3. Cumulative intrudable pore volume from MIP experiments

The Figure S.1 below shows the cumulative curves measured with MIP of all studied mixes. The results from mix P4 display the mix with the lowest cumulative volume and WQ the mix with the largest cumulative volume.

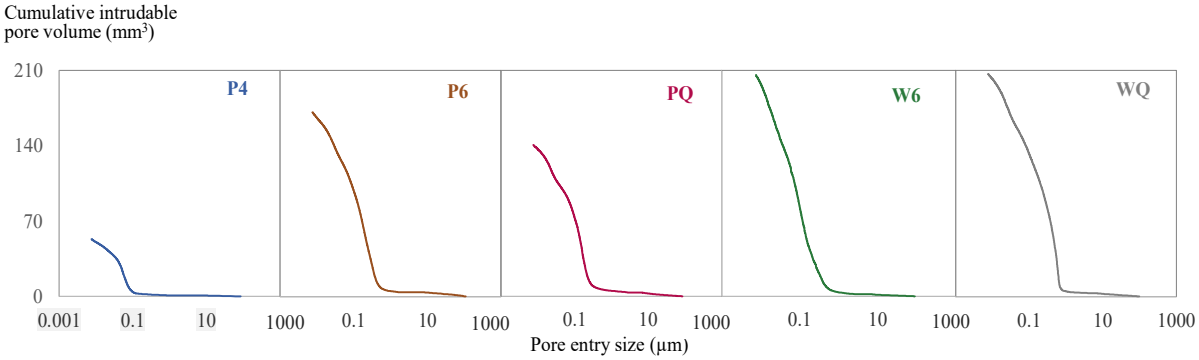

Figure S.1. Cumulative intrudable pore volume from MIP experiments.

References

[1] Y.A. Villagrán Zaccardi, N.M. Alderete, N. De Belie, Improved model for capillary absorption in cementitious materials: Progress over the fourth root of time, Cem Concr Res 100 (2017) 153–165. https://doi.org/10.1016/j.cemconres.2017.07.003.

[2] C. Hall, Anomalous diffusion in unsaturated flow: Fact or fiction?, Cem Concr Res 37 (2007) 378–385. https://doi.org/10.1016/j.cemconres.2006.10.004.

[3] F. Ren, C. Zhou, Q. Zeng, Z. Zhang, U. Angst, W. Wang, Quantifying the anomalous water absorption behavior of cement mortar in view of its physical sensitivity to water, Cem Concr Res 143 (2021) 106395. https://doi.org/10.1016/j.cemconres.2021.106395.

[4] C. Hall, Capillary imbibition in cement-based materials with time-dependent permeability, Cem Concr Res 124 (2019). https://doi.org/10.1016/j.cemconres.2019.105835.

[5] N.M. Alderete, Y.A. Villagrán Zaccardi, N. De Belie, Physical evidence of swelling as the cause of anomalous capillary water uptake by cementitious materials, Cem Concr Res 120 (2019) 256–266. https://doi.org/10.1016/j.cemconres.2019.04.001.

[6] C. Zhou, X. Zhang, Z. Wang, Z. Yang, Water sensitivity of cement-based materials, Journal of the American Ceramic Society 104 (2021) 4279–4296. https://doi.org/10.1111/jace.17918.

[7] N.M. Alderete, A. Mignon, K. Schollbach, Y. Villagrán-Zaccardi, Deformations in cement pastes during capillary imbibition and their relation to water and isopropanol as imbibing liquids, Materials 15 (2022). https://doi.org/10.3390/ma15010036.

[8] N.M. Alderete, Y.A. Villagrán Zaccardi, N. De Belie, Physical evidence of swelling as the cause of anomalous capillary water uptake by cementitious materials, Cem Concr Res 120 (2019) 256–266. https://doi.org/10.1016/j.cemconres.2019.04.001.

[9] H. Chemmi, D. Petit, V. Tariel, J.P. Korb, R. Denoyel, R. Bouchet, P. Levitz, A comprehensive multiscale moisture transport analysis: From porous reference silicates to cement-based materials, European Physical Journal: Special Topics 224 (2015) 1749–1768. https://doi.org/10.1140/epjst/e2015-02496-5.

[10] Z.L. Jiang, Y.J. Pan, J.F. Lu, Y.C. Wang, Pore structure characterization of cement paste by different experimental methods and its influence on permeability evaluation, Cem Concr Res 159 (2022) 106892. https://doi.org/10.1016/j.cemconres.2022.106892.

[11] R. Schulte Holthausen, M. Raupach, Monitoring the internal swelling in cementitious mortars with single-sided 1H nuclear magnetic resonance, Cem Concr Res 111 (2018) 138–146. https://doi.org/10.1016/j.cemconres.2018.05.021.

[12] N. Fischer, R. Haerdtl, P.J. McDonald, Observation of the redistribution of nanoscale water filled porosity in cement based materials during wetting, Cem Concr Res 68 (2015) 148–155. https://doi.org/10.1016/j.cemconres.2014.10.013.

[13] P.J. McDonald, O. Istok, M. Janota, M. Agata, D.A. Faux, Sorption , anomalous water transport and dynamic porosity in cement paste : a spatially localised 1 H NMR relaxation study and a proposed mechanism, Cem Concr Res 133 (2020) 106045. https://doi.org/10.1016/j.cemconres.2020.106045.

[14] A.M. Gajewicz, E. Gartner, K. Kang, P.J. McDonald, V. Yermakou, A 1H NMR relaxometry investigation of gel-pore drying shrinkage in cement pastes, Cem Concr Res 86 (2016) 12–19. https://doi.org/10.1016/j.cemconres.2016.04.013.

[15] P. Zhang, F.H. Wittmann, P. Lura, H.S. Müller, S. Han, T. Zhao, Application of neutron imaging to investigate fundamental aspects of durability of cement-based materials: A review, Cem Concr Res 108 (2018) 152–166. https://doi.org/10.1016/j.cemconres.2018.03.003.

[16] N. Alderete, Y. Villagrán Zaccardi, D. Snoeck, B. Van Belleghem, P. Van den Heede, K. Van Tittelboom, N. De Belie, Capillary imbibition in mortars with natural pozzolan, limestone powder and slag evaluated through neutron radiography, electrical conductivity, and gravimetric analysis, Cem Concr Res 118 (2019) 57–68. https://doi.org/10.1016/j.cemconres.2019.02.011.

[17] Z. Hu, T. Cajuhi, N. Toropovs, M. Griffa, M. Wyrzykowski, A. Kaestner, L. De Lorenzis, P. Lura, A neutron radiography study on the drying of cement mortars: Effect of mixture composition and crack length, Cem Concr Res 172 (2023). https://doi.org/10.1016/j.cemconres.2023.107245.

[18] S. Didier, A. Natalia, B. Van Belleghem, P. Van DeN Heede, K. Van Tittelboom, N. De Belie, Internal curing of cement pastes by superabsorbent polymers studied by means of neutron radiography, in: G. De Schutter, N. De Belie, A. Janssens, N. Van Den Bossche (Eds.), XIV DBMC 2017 Conference, RILEM, Paris, 2017.

[19] D. Snoeck, P. Van den Heede, T. Van Mullem, N. De Belie, Water penetration through cracks in self-healing cementitious materials with superabsorbent polymers studied by neutron radiography, Cem Concr Res 113 (2018) 86–98. https://doi.org/10.1016/j.cemconres.2018.07.002.

[20] P. Van den Heede, B. Van Belleghem, N. Alderete, K. Van Tittelboom, N. De Belie, Neutron radiography based visualization and profiling of water uptake in (Un)cracked and autonomously healed cementitious materials, Materials 9 (2016). https://doi.org/10.3390/ma9050311.

[21] Z.P. Bazant, L.J. Najjar, Nonlinear water diffusion in non-saturated concrete, Mater Struct 25 (1972) 3–20.

[22] M. Mainguy, O. Coussy, V. Baroghel-Bouny, Role of Air Pressure in Drying of Weakly Permeable Materials, J Eng Mech 127 (2001) 582–592. https://doi.org/10.1061/(ASCE)0733-9399(2001)127:6(582).

[23] F. Ren, C. Zhou, Q. Zeng, Z. Zhang, U. Angst, W. Wang, Quantifying the anomalous water absorption behavior of cement mortar in view of its physical sensitivity to water, Cem Concr Res 143 (2021). https://doi.org/10.1016/j.cemconres.2021.106395.

[24] Z. Zhang, U. Angst, A Dual-Permeability Approach to Study Anomalous Moisture Transport Properties of Cement-Based Materials, Transp Porous Media 135 (2020) 59–78. https://doi.org/10.1007/s11242-020-01469-y.

[25] C. Hall, Capillary imbibition in cement-based materials with time-dependent permeability, Cem Concr Res 124 (2019). https://doi.org/10.1016/j.cemconres.2019.105835.

[26] R. Snellings, J. Chwast, Ö. Cizer, N. De Belie, Y. Dhandapani, P. Durdzinski, J. Elsen, J. Haufe, D. Hooton, C. Patapy, M. Santhanam, K. Scrivener, D. Snoeck, L. Steger, S. Tongbo, A. Vollpracht, F. Winnefeld, B. Lothenbach, RILEM TC-238 SCM recommendation on hydration stoppage by solvent exchange for the study of hydrate assemblages, Materials and Structures/Materiaux et Constructions 51 (2018). https://doi.org/10.1617/s11527-018-1298-5.

[27] N.V.Y. Scarlett, I.C. Madsen, Quantification of phases with partial or no known crystal structures, Powder Diffr 21 (2006) 278–284. https://doi.org/10.1154/1.2362855.

[28] E.H. Lehmann, P. Vontobel, L. Wiezel, Properties of the radiography facility NEUTRA at SINQ and its potential for use as European reference facility NDT&E, Nondestructive Testing and Evaluation 16 (2001) 191–202. https://doi.org/10.1080/10589750108953075.

[29] B. Blau, K.N. Clausen, S. Gvasaliya, M. Janoschek, S. Janssen, L. Keller, B. Roessli, J. Schefer, P. Tregenna-Piggott, W. Wagner, O. Zaharko, The Swiss Spallation Neutron Source SINQ at Paul Scherrer Institut, Neutron News 20 (2009) 5–8. https://doi.org/10.1080/10448630903120387.

[30] C. Carminati, M. Strobl, A. Kaestner, KipTool, a general purpose processing tool for neutron imaging data, SoftwareX 10 (2019) 100279. https://doi.org/10.1016/j.softx.2019.100279.

[31] P. Boillat, C. Carminati, F. Schmid, C. Grünzweig, J. Hovind, A. Kaestner, D. Mannes, M. Morgano, M. Siegwart, P. Trtik, P. Vontobel, E.H. Lehmann, Chasing quantitative biases in neutron imaging with scintillator-camera detectors: a practical method with black body grids, Opt Express 26 (2018) 15769. https://doi.org/10.1364/oe.26.015769.

[32] C. Carminati, P. Boillat, F. Schmid, P. Vontobel, J. Hovind, M. Morgano, M. Raventos, M. Siegwart, D. Mannes, C. Gruenzweig, P. Trtik, E. Lehmann, M. Strobl, A. Kaestner, Implementation and assessment of the black body bias correction in quantitative neutron imaging, PLoS One 14 (2019) 1–24. https://doi.org/10.1371/journal.pone.0210300.

[33] R. Schulte Holthausen, M. Raupach, Monitoring the internal swelling in cementitious mortars with single-sided 1H nuclear magnetic resonance, Cem Concr Res 111 (2018) 138–146. https://doi.org/10.1016/j.cemconres.2018.05.021.

[34] A.M. Gajewicz, E. Gartner, K. Kang, P.J. McDonald, V. Yermakou, A 1H NMR relaxometry investigation of gel-pore drying shrinkage in cement pastes, Cem Concr Res 86 (2016) 12–19. https://doi.org/10.1016/j.cemconres.2016.04.013.

[35] S. Diamond, Mercury porosimetry. An inappropriate method for the measurement of pore size distributions in cement-based materials, Cem Concr Res 30 (2000) 1517–1525. https://doi.org/10.1016/S0008-8846(00)00370-7.

[36] N. Alderete, Y. Villagrán, A. Mignon, D. Snoeck, N. De Belie, Pore structure description of mortars containing ground granulated blast-furnace slag by mercury intrusion porosimetry and dynamic vapour sorption, Constr Build Mater 145 (2017) 157–165. https://doi.org/10.1016/j.conbuildmat.2017.03.245.

[37] P.K. Mehta, P.J.M. Monteiro, Concrete : structure, properties and materials., 2nd ed., Englewood Cliffs (N.J.) : Prentice-Hall, 1993., 1993.

[38] Mindness Sidney, Concrete, 2nd ed., Prentice Hall, 1992.

[39] Y. Wang, L. Li, M. An, Y. Sun, Z. Yu, H. Huang, Factors Influencing the Capillary Water Absorption Characteristics of Concrete and Their Relationship to Pore Structure, Applied Sciences (Switzerland) 12 (2022). https://doi.org/10.3390/app12042211.

[40] H. Ma, Mercury intrusion porosimetry in concrete technology: tips in measurement, pore structure parameter acquisition and application, Journal of Porous Materials 21 (2014) 207–215. https://doi.org/10.1007/s10934-013-9765-4.

[41] J. Adolphs, M.J. Setzer, P. Heine, Changes in pore structure and mercury contact angle of hardened cement paste depending on relative humidity, 2002.

[42] Y. Zhang, B. Yang, Z. Yang, G. Ye, Ink-bottle effect and pore size distribution of cementitious materials identified by pressurization-depressurization cycling mercury intrusion porosimetry, Materials 12 (2019). https://doi.org/10.3390/ma12091454.

[43] J.J. Thomas, H.M. Jennings, Changes in the size of pores during shrinkage (or expansion) of cement paste and concrete, Cem Concr Res 33 (2003) 1897–1900. https://doi.org/10.1016/S0008-8846(03)00167-4.

[44] H.F.W. Taylor, Cement Chemistry, 2nd ed., London, UK, 1997.

[45] A. Bede, A. Scurtu, I. Ardelean, NMR relaxation of molecules confined inside the cement paste pores under partially saturated conditions, Cem Concr Res 89 (2016) 56–62. https://doi.org/10.1016/j.cemconres.2016.07.012.

[46] M. Reyssat, L. Courbin, E. Reyssat, H.A. Stone, Imbibition in geometries with axial variations, J Fluid Mech 615 (2008) 335–344. https://doi.org/10.1017/S0022112008003996.

[47] B. Yang, L. You, J. Yang, H. Han, L. Wang, Pore Shape Factors in Shale: Calculation and Impact Evaluation on Fluid Imbibition, 2018.

[48] M. Hallaji, A. Seppänen, M. Pour-Ghaz, Electrical resistance tomography to monitor unsaturated moisture flow in cementitious materials, Cem Concr Res 69 (2015) 10–18. https://doi.org/10.1016/j.cemconres.2014.11.007.

[49] L. De Brabandere, N.M. Alderete, N. De Belie, Capillary Imbibition in Cementitious Materials: Effect of Salts and Exposure Condition, Materials 15 (2022). https://doi.org/10.3390/ma15041569.

[50] Y.A. Villagrán-Zaccardi, N.M. Alderete, A. Benítez, M.F. Carrasco, P. Corallo, R. López, C. Rios, Relationship between sorptivity coefficients of concrete as calculated from the evolution of water uptake versus t0.5 or t0.25, Constr Build Mater 342 (2022). https://doi.org/10.1016/j.conbuildmat.2022.128084.

[51] N.M. Alderete, Y.A. Villagrán Zaccardi, N. De Belie, Mechanism of long-term capillary water uptake in cementitious materials, Cem Concr Compos 106 (2020). https://doi.org/10.1016/j.cemconcomp.2019.103448.

[52] C. Hall, A. Hamilton, Beyond the Sorptivity : Definition , Measurement , and Properties of the Secondary Sorptivity, Journal of Materials in Civil Engineering 30 (2018) 1–7. https://doi.org/10.1061/(ASCE)MT.1943-5533.0002226.

[53] F. Huang, Z. Hu, H. Li, Y. Wang, J. Liu, Deformation mechanisms of cement paste with ultra-low water-to-cement ratios under different curing conditions at early ages, Constr Build Mater 364 (2023). https://doi.org/10.1016/j.conbuildmat.2022.129951.

[54] N.M. Alderete, Y.A. Villagrán Zaccardi, N. De Belie, Physical evidence of swelling as the cause of anomalous capillary water uptake by cementitious materials, Cem Concr Res 120 (2019) 256–266. https://doi.org/10.1016/j.cemconres.2019.04.001.

[55] F. Huang, Z. Hu, S. Li, J. Liu, F. Han, J. Liu, Long-term deformation and mechanical properties evolution of cement paste with ultra-low water-to-cement ratio driven by water migration, Journal of Building Engineering (2023) 107250. https://doi.org/10.1016/j.jobe.2023.107250.

[56] Z. Zhang, U. Angst, Modeling anomalous moisture transport in cement-based materials with kinetic permeability, Int J Mol Sci 21 (2020). https://doi.org/10.3390/ijms21030837.

[57] J.E. Guyer, D. Wheeler, J.A. Warren, FiPy: Partial Differential Equations with Python, (n.d.). https://doi.org/doi:10.1109/MCSE.2009.52.

[58] R. Storn, K. Price, Differential Evolution-A Simple and Efficient Heuristic for Global Optimization over Continuous Spaces, Kluwer Academic Publishers, 1997.